lows. On Chirasil-Val columns, the amino acid enantiomer having the same α-carbon configuration as the Val moiety of the chromatographic phase typically has the longer retention time of the pair [E. Bayer, *Z. Naturforsch. B* **38**, 1281 (1983)]. This expectation was verified for the 2-a-2,3-dmpa stereoisomers by preparing the *N*-chloroacetyl derivatives of a synthetic standard containing all four stereoisomers and partially digesting this standard with hog kidney acylase I, which specifically hydrolyzes the amide linkages of L enantiomers [C. G. Baker, S. J. Fu, S. M. Birnbaum, H. A. Sober, J. P. Greenstein, *J. Am. Chem. Soc.* **74**, 4701 (1952)]. One of the resulting free L amino acids and the four residual unhydrolyzed *N*-chloroacetyl stereoisomers were isolated from the reaction mixture, the latter was acid hydrolyzed, and both preparations rechromatographed on the Chirasil-L-Val and Chirasil-D-Val phases after appropriate derivatization. The expected behavior was observed, that is, two diminished peaks (L) from the residual chloroacetylated stereoisomers corresponding in retention times to those expected for the L enantiomers and a corresponding match of the isolated free amino acid (L) with the expected L-enantiomer retention time of the (2*S*,3*S*-2*R*,3*R*) pair. The (2*S*,3*S*-2*R*,3*R*) and (2*S*,3*R*-2*R*,3*S*) diastereomer pairs of 2-a-2,3-dmpa were identified from the chemical shifts of their α-methyl groups observed in proton nuclear magnetic resonance (NMR) spectra of the methyl esters ($CDCl_3$) and comparison with literature values for the corresponding (2*S*,3*S*)- and (2*R*,3*S*)-2-a-2,3-dmpa methyl esters [U. Schöllkopf, R. Tölle, E. Egert, M. Nieger, *Liebigs Ann. Chem.* **1987**, 399 (1987)]. The diastereomer pairs were present in the standard in different amounts and thus, the GC-MS chromatograms and the NMR spectrum could be correlated.

12. J. R. Cronin, W. E. Gandy, S. Pizzarello, *J. Mol. Evol.* **17**, 265 (1981).
13. J. Ipsen and P. Feigl, *Barcroft's Introduction to Biostatistics* (Harper & Row, New York, ed. 2, 1970).
14. J. L. Bada, M. Zhao, S. Steinberg, E. Ruth, *Nature* **319**, 314 (1986).
15. J. R. Cronin, S. Pizzarello, G. U. Yuen, *Geochim. Cosmochim. Acta* **49**, 2259 (1985).
16. J. G. Lawless and M. S. Chadha, *Anal. Biochem.* **44**, 473 (1971).
17. J. R. Cronin, G. U. Yuen, S. Pizzarello, *ibid.* **124**, 139 (1982).
18. K. R. Leimer, R. H. Rice, C. W. Gehrke, *J. Chromatogr.* **141**, 121 (1977); E. Gelpi, W. A. Koenig, J. Gibert, J. Oró, *J. Chromatogr. Sci.* **7**, 604 (1969).
19. Four amino acids were analyzed in this work in addition to the two diastereomers of 2-a-2,3-dmpa. 2-Methyl norvaline has no known natural terrestrial source. Isovaline has been found in fungal antibiotics [H. Brückner, J. Maisch, C. Reinecke, A. Kimonyo, *Amino Acids* **1**, 251 (1991)]. Norvaline has been reported in an antifungal peptide produced by *Bacillus subtilis* [P. Nandi and G. P. Sen, *Nature* **171**, 871 (1953)] and as an isoleucine fermentation product [M. Kisumi, M. Sugiura, I. Chibata, *J. Biochem.* **80**, 333 (1976)]. α-Amino-*n*-butyric acid is the most widely distributed, occurring in vertebrate physiological fluids and in plants.
20. J. L. Bada, *Philos. Trans. R. Soc. London Ser. B* **333**, 349 (1991).
21. J. R. Cronin and S. Pizzarello, *Adv. Space Res.* **3**, 5 (1983).
22. E. Rubenstein, W. A. Bonner, H. P. Noyes, G. S. Brown, *Nature* **306**, 118 (1983); W. A. Bonner and E. Rubenstein, *Biosystems* **20**, 99 (1987).
23. J. M. Greenberg, in *Physical Origin of Homochirality in Life*, D. B. Cline, Ed. (American Institute of Physics, New York, 1996), pp. 185–210.
24. J. J. Flores, W. A. Bonner, G. A. Massey, *J. Am. Chem. Soc.* **99**, 3622 (1977).
25. J. R. Cronin, G. W. Cooper, S. Pizzarello, *Adv. Space Res.* **15**, 91 (1995).
26. S. Epstein, R. V. Krishnamurthy, J. R. Cronin, S. Pizzarello, G. U. Yuen, *Nature* **326**, 477 (1987).
27. E. T. Peltzer and J. L. Bada, *ibid.* **272**, 443 (1978); J. R. Cronin, S. Pizzarello, R. V. Krishnamurthy, S. Epstein, *Geochim. Cosmochim. Acta* **57**, 4745 (1993).
28. This result is analogous to the α-epimerization of L-isoleucine (2*S*,3*S*), which gives D-alloisoleucine (2*R*,3*S*); however, in the case of a Strecker synthesis, the 2*S*-2*R* equilibrium is achieved by formation of the chiral center rather than by inversion of the configuration at an existing chiral center. As envisioned here, the C-3 of 2-a-2,3-dmpa would not necessarily have been homochiral as in the case of biological isoleucine, but might have had only a modest enantiomeric excess. Consequently, excesses of the D and L enantiomers of the respective diastereomers would also have been small.
29. Y. Miao, L. E. Snyder, Y.-J. Kuan, F. J. Lovas, *Bull. Am. Astron. Soc.* **26**, 906 (1994); F. Coombes, N.-Q. Rieu, G. Wlodarczak, *Astron. Astrophys.* **308**, 618 (1995).
30. A. J. MacDermott, in *Chemical Evolution: Physics of the Origin and Evolution of Life*, J. Chela-Flores and F. Raulin, Eds. (Kluwer, New York, 1996), pp. 373–379.
31. See G. Wald, *Ann. N.Y. Acad. Sci.* **69**, 353 (1957), and the experimental work reviewed by Bonner (1).
32. We thank C. Moore of the Arizona State University Center for Meteorite Studies for a sample of the Murchison meteorite; M. Madison for calculation of the isomer numbers using the program ASSEMBLE [B. D. Christie and M. E. Munk, *Anal. Chim. Acta* **200**, 347 (1987)]; R. Nieman for help in obtaining and interpreting NMR spectra; J. Bada, K. Kvenvolden, and an anonymous reviewer for constructive reviews of the manuscript; and the NASA Exobiology Program for research support (NAGW-1899).

9 October 1996; accepted 15 January 1997

Atomistic Simulation of Shock Wave–Induced Melting in Argon

A. B. Belonoshko

A three-dimensional molecular dynamics simulation of shock wave loading was undertaken to investigate the Hugoniot equation of state at the transition of argon from solid to liquid. The simulated data agree with shock wave and static high-pressure experimental data. The melting transition in this simulation occurs without overshooting the argon melting temperature. There are two discontinuities that may bracket a mixed-phase region of solid and liquid along the simulated argon Hugoniot. This is an intrinsic feature of the Hugoniot crossing the argon melting curve and does not require the addition of any solid-solid phase transition.

Shock wave experiments are particularly well suited for molecular dynamic (MD) simulations because in such experiments sample sizes are small and time scales are short (1). Few studies have been devoted to the simulation of shock wave–induced phase transitions (2), and none of them were done in three dimensions. I have simulated the shock wave–induced melting transition for Ar, an element for which many physical parameters are well known and for which I have simulated the melting curve (3), which agrees with experimental data (4). Argon transforms to liquid directly from the face-centered-cubic (fcc) phase without any high-pressure and high-temperature solid-solid phase transformations (5).

The initial configuration for the simulation consisted of Ar atoms in an fcc lattice with n by n by m unit cells translated in x, y, and z directions, respectively, with n varying from 5 to 10 and m varying from 60 to 120 in different simulations. The minimum number of atoms was 6000, and the maximum was 48,000. Calculations with different numbers of atoms showed that 6000 atoms is sufficient to obtain reliable results. Periodic boundary conditions were applied in the x and y directions. An Ar-Ar interaction was described in terms of the Buckingham potential (3, 6, 7). The shock wave was generated through the motion of a piston in the $-z$ direction with a given velocity (U_p). The interaction of the Ar atom with the piston was calculated on the assumption that a piston is a solid homogeneous Ar crystal. On the side of the sample opposite the piston (at $z = 0$) Ar atoms interacted with the elastic wall. The time step for solving equations of motion was 4 fs, and the number of time steps varied from 3000 to 6000. I cross-checked all calculations, using simulations with various time, time step, length of sample, cutoff radius of interaction, cross-sectional area, number of atoms, and initial conditions.

The propagation of the shock wave front was observed in snapshots of the structure (a supplementary figure is available to online subscribers at http://www.sciencemag.org), allowing rather precise (error less than 1%) measurement of the shock wave velocity (U_s). To measure the sound velocity V_s in the shock-compressed part of the sample, I stopped the piston at some time step (usually time step 1000) and measured the velocity of the rarefaction wave. Pressure profiles were used to determine U_s and V_s (8). Volume (V), pressure (P), and temperature (T) were monitored as a function of z. I also calculated P and V from U_p-U_s data using two of the Rankine-Hugoniot (RH) relations:

Theoretical Geochemistry Program, Institute of Earth Sciences, Uppsala University, S-752 36, Uppsala, Sweden.

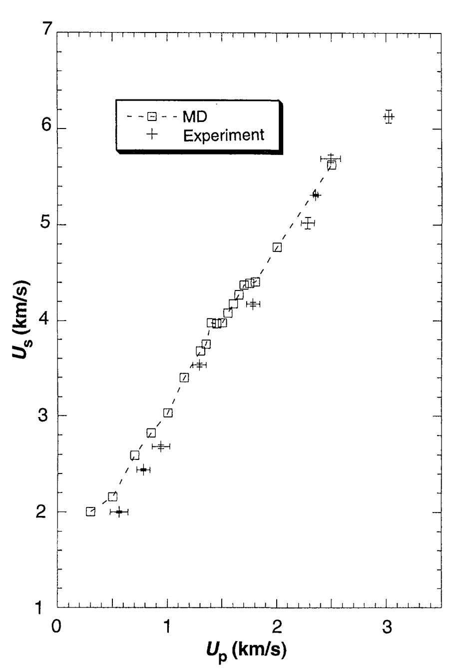

Fig. 1. Simulated shock wave velocity (U_s) as a function of particle velocity (U_p) compared to experimental data (shown with error bars) (*11*).

$$V = V_0\left(1-\frac{U_p}{U_s}\right) \qquad (1)$$

and

$$P = \rho_0 U_p U_s + P_0 \qquad (2)$$

The initial state (denoted by the "0" subscript) was at $T = 5$ K and a density (ρ_0) of 1.784 g/cm^3 ($V_0 = 22.413$ cm^3/mol). The initial pressure P_0 was close to 1 bar and can be neglected, because the first term on the right in Eq. 2 is much larger.

Shock waves were simulated in the range 0.3 km/s $< U_p <$ 2.5 km/s. At $U_p <$ 1.0 km/s the calculated U_s values are somewhat larger than the experimental values (Fig. 1). This is due to the higher initial density in my simulations (1.784 versus 1.65 g/cm^3) and to the fact that the simulated crystal is the ideal crystal whereas the experimental one is polycrystalline. The analysis of structures (*9*) at U_p $<$ 1.0 km/s shows that the shock wave produces micrograins of Ar, similar to the grains observed in other simulations (*1*). The Hugoniot elastic limit is exceeded at $U_p \geq$ 0.85 km/s. The calculated U_p-U_s data agree with experiment (Fig. 1). The P and V values behind the shock wave front calculated from time averages of V and P [as done, for example, in (*10*)] derived directly from simulations and from the RH relations (Eqs. 1 and 2) are in good agreement with experimental values (*3, 6, 7, 11*).

Temperature can be calculated directly in a computer simulation, for the velocities of atoms are known at each time step (*10*). The curve of P versus T (Fig. 2A) derived from the simulations agrees with the experimental data. There is a change in the slope of the P-T curve, which represents a mixture of solid and liquid phases existing in different areas of the sample behind the shock waves at the same time. When the solid Hugoniot arrives at the P and T conditions of melting at some U_p, a small increase in U_p does not provide sufficient energy to permit the sample to jump to the liquid branch of the Hugoniot because of the finite enthalpy of melting. Instead, as U_p increases, larger parts of the shocked sample transform into the liquid state. Analysis of structures (*9*) shows that some parts of the system are liquid whereas others remain solid. Some points in the transitional regime fall in between the solid and liquid volumes (Fig. 2B), indicating the coexistence of two phases. Analysis of the structure also shows that melting occurs without any so-called "overshooting" (when a substance metastably remains solid even when its temperature is higher than the melting temperature), which is often used to explain the discrepancy between static and shock wave experiments. The melting curve of Ar calculated in static simulation (*3*) passes through the solid-liquid transition range of the Hugoniot (Fig. 2A).

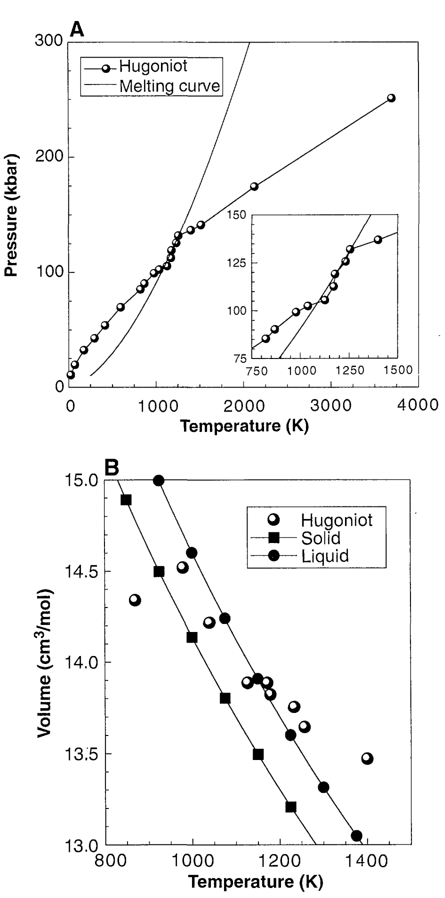

Fig. 2. (**A**) Calculated pressures and temperatures along the Hugoniot compared with the melting curve calculated with the same interatomic potential. The discontinuous Hugoniot behavior coincides with the melting point. There is a substantial pressure interval in which the Hugoniot follows the pressure and temperature of melting. This interval is shown in the magnified portion of the figure. (**B**) The volume of Ar along the Hugoniot compared with the volumes of solid and liquid Ar along the melting curve. Some of the Hugoniot volume falls into the intermediate range between the volumes of solid and liquid Ar, indicating the coexistence of solid and liquid phases in the Hugoniot transition regime.

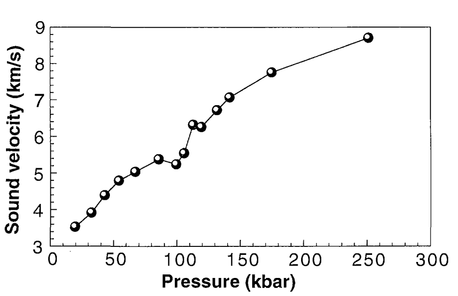

Fig. 3. Sound velocity versus pressure along the Ar Hugoniot. The dependence exhibits two discontinuities separated by $\Delta U_p \approx$ 0.4 km/s (compare with Fig. 1).

The calculated dependence of V_s on pressure for Ar (Fig. 3) is qualitatively similar to the dependence measured for Fe (*12*) (both elements have two discontinuities and in both cases these discontinuities are separated by ~0.4 km/s in terms of U_p). These simulations of the Ar Hugoniot suggest that these discontinuities may be related to melting rather than to a solid-solid phase transition. This may have important implications for Fe. It has been suggested (*12*) that the first discontinuity for Fe is related to a solid-solid transition and the second one to melting. My simulations suggest that these two discontinuities may represent a mixed-phase region of solid and liquid due to the melting of Fe. Although the possible existence of an ultrahigh-PT Fe phase is definitely an open question, it is possible that the two discontinuities on the sound V-P curve (*12*) are not evidence of a solid-solid transition (*13*).

REFERENCES AND NOTES

1. B. L. Holian, *Shock Waves* **5**, 149 (1995).
2. D. H. Robertson, D. W. Brenner, C. T. White, *Phys. Rev. Lett.* **67**, 3132 (1991).
3. A. B. Belonoshko, *High Pressure Res.* **10**, 583 (1992), and references therein.
4. A. P. Jephcoat and S. P. Besedin, *Philos. Trans. R. Soc. London Ser. A* **354**, 1333 (1996).
5. S. M. Stishov, I. N. Makarenko, V. A. Ivanov, V. I. Fedosimov, *JETP Lett.* **11**, 13 (1970).
6. M. Ross, *Phys. Rev. A* **8**, 1466 (1973).
7. ———, H. K. Mao, P. M. Bell, J. A. Xu, *J. Chem. Phys.* **85**, 1028 (1986).
8. The pressure profiles allow one to determine the positions of shock and rarefaction waves at every time step; knowing the number of the time step and its size, one can calculate the corresponding velocity from the formula $v = (z_{t2} - z_{t1})/(t_2 - t_1)$, where z represents the positions of the corresponding wave, and t_2 and t_1 are different times of measurement. The quantity z can be measured with a precision of a few

angstroms. Therefore, the magnitude of ν can be determined as precisely as needed by choosing a sufficiently large time interval $(t_2 - t_1)$ between the corresponding measurements of z.
9. Analysis of structures means that the structures were animated by the use of the Xmol program. Visual inspection of snapshots (similar to those available to online subscribers at http://www.sciencemag.org) allowed me to distinguish between solid and liquid structures. This procedure was successfully applied in the determination of the melting curve of MgO [A. Belonoshko and L. S. Dubrovinsky, *Am. Mineral.* **81**, 303 (1996)], and in the case of a monatomic substance it is even more reliable.
10. V. Y. Klimenko and A. N. Dremin, in *Detonatsija*, O. N. Breusov, Ed. (Akademii Nauk, Moscow, 1978), p. 79.
11. R. D. Dick, R. H. Warnes, J. Skalyo, *J. Chem. Phys.* **53**, 1648 (1970).
12. J. M. Brown and R. G. McQueen, *J. Geophys. Res.* **91**, 7485 (1986).
13. R. Boehler suggested in his talk at the Structure of Earth Deep Interior VI Symposium (July 1996) that Brown and McQueen (*12*) observed only one discontinuity and that this discontinuity is related to melting. According to the results of my study, it is likely that indeed two discontinuities were observed.
14. I am grateful to O. L. Anderson, M. Brown, and F. Seifert for helpful discussions. Comments by two anonymous reviewers were useful. Simulations were done with the use of the IBM SP2 in the Parallel Computer Center in Stockholm. The research was supported by Swedish Natural Science Council (Naturvetenskapliga Forskninrådet) grant G-Gu 06901-301.

25 September 1996; accepted 30 December 1996

Twentieth-Century Sea Surface Temperature Trends

Mark A. Cane,* Amy C. Clement, Alexey Kaplan,
Yochanan Kushnir, Dmitri Pozdnyakov, Richard Seager,
Stephen E. Zebiak, Ragu Murtugudde

An analysis of historical sea surface temperatures provides evidence for global warming since 1900, in line with land-based analyses of global temperature trends, and also shows that over the same period, the eastern equatorial Pacific cooled and the zonal sea surface temperature gradient strengthened. Recent theoretical studies have predicted such a pattern as a response of the coupled ocean-atmosphere system to an exogenous heating of the tropical atmosphere. This pattern, however, is not reproduced by the complex ocean-atmosphere circulation models currently used to simulate the climatic response to increased greenhouse gases. Its presence is likely to lessen the mean 20th-century global temperature change in model simulations.

Amidst the often contentious debate on global warming, there are areas of general consensus. There is agreement that Earth's surface temperature has increased over the last 100 years by between $\sim$0.3° and 0.6°C (*1*). There is, however, disagreement as to the causes of this temperature increase. It may be a response to anthropogenic forcing, a part of the climate system's innate natural variability, or a combination of the two. There is also general consensus that the radiative effect of increased atmospheric concentrations of greenhouse gases will cause Earth's temperature to rise. The direct warming effect of these gases is rather small, but there is a potential for amplification by positive feedbacks within the climate system. Understanding of these mechanisms is incomplete, and the strength of the amplification is uncertain, as evidenced by the fact that, when loaded with twice the modern concentration of atmospheric CO_2, state-of-the-art climate models give mean global changes varying from 1.5° to 4.5°C (*1*).

Until quite recently, simulations of the climatic response to increasing concentrations of greenhouse gases gave temperature changes that exceeded the observed increase by about a factor of 2 (*1*, *2*). It was then suggested that the discrepancy might result from the neglect of the cooling effect of sulfate aerosols (*3*). Inclusion of this effect brought simulations into better agreement with observations (*1*, *2*). Unfortunately, the radiative effects of aerosols are poorly understood. It is quite possible that the influence of the values currently used in simulations is considerably larger than the true influence (*4*) and is substituting for natural moderating mechanisms that are absent or underrepresented in present models.

Here we point out a pattern in the changes of sea surface temperature (SST) over the course of the 20th century—an increase in the zonal gradient across the equatorial Pacific—that has been missed in simulations performed with comprehensive climate models [general circulation models (GCMs)]. Recent theoretical studies (*5*–*8*) have predicted this pattern as a response to exogenous heating of the tropical atmosphere. If the theory is correct, it would provide evidence that the coupled atmosphere-ocean dynamics are delaying, and possibly regulating, global warming. The absence of this mechanism in the GCM simulations may account in part for the discrepancy between the observed and modeled global mean temperature rise.

The theoretical ideas we invoke (*5*–*8*) follow the line of argument first proposed by Bjerknes (*9*), which forms the foundation of our present understanding of the El Niño–Southern Oscillation (ENSO) phenomenon (*10*). Suppose a uniform external heating is imposed on the tropical Pacific. The SST will tend to rise, leading to increased evaporative cooling until a new, warmer equilibrium is reached. This change would be the only response in the absence of a decisive contribution from ocean dynamics. In the eastern equatorial region, however, vigorous upwelling brings up cold waters from below, counteracting the warming tendency. Thus, initially, the SST increases more in the west than in the east, enhancing the temperature gradient along the equator. The atmosphere responds with increasing trade winds, which in turn will increase the upwelling rate and the thermocline (*11*) tilt, cooling the surface waters in the east and further enhancing the temperature contrast. As a consequence of this dynamical feedback, the mean temperature will increase less than it would with the purely thermodynamic response.

To test the mechanism, we imposed a uniform forcing on a simplified model of the ocean-atmosphere system in the tropical Pacific, the Lamont model used to forecast El Niño (*12*). The forcing was chosen so that in the absence of ocean dynamics, SST would increase by 1°C everywhere. In the model's mean annual response (Fig. 1), not only does the eastern equatorial Pacific cool, consistent with the mechanism described above, but the dynamics of the coupled ocean atmosphere system spreads the influence of the upwelled waters throughout the tropical Pacific, such that the mean increase in temperature is only 0.5°C.

A number of objections to this theory and model demonstration may be raised. The theory relies on colder upwelled waters balancing some of the imposed heat input, but the simple ocean model used specifies a fixed thermocline temperature. In reality, the waters of the equatorial thermocline originate at the surface at higher latitudes. If these source waters were to warm up, then equatorial thermocline temperatures would eventually increase; the cooling effect would then be reduced on a time scale set by the renewal time for the equatorial thermocline. Some recent

---

M. A. Cane, A. C. Clement, A. Kaplan, Y. Kushnir, D. Pozdnyakov, R. Seager, S. E. Zebiak, Lamont-Doherty Earth Observatory, Palisades, NY 10964–8000, USA.
R. Murtugudde, Universities Space Research Association, Laboratory for Hydrospheric Processes, NASA Goddard Space Flight Center, Greenbelt, MD 20771, USA.

*To whom correspondence should be addressed.